ORIGINAL ARTICLE

Open Access

Cutting Behavior of Cortical Bone in Different Bone Osteon Cutting Angles and Depths of Cut

Yuanqiang Luo[1,2], Yinghui Ren[1*], Yang Shu[1], Cong Mao[2], Zhixiong Zhou[1] and Z. M. Bi[3]

Abstract

Cortical bone is semi-brittle and anisotropic, that brings a challenge to suppress vibration and avoid undesired fracture in precise cutting process in surgeries. In this paper, a novel analytical model is proposed to represent cortical bone cutting processes. The model is utilized to predict the chip formations, material removal behavior and cracks propagation under varying bone osteon cutting angles and depths. Series of orthogonal cutting experiments were conducted on cortical bone to investigate the impact of bone osteon cutting angle and depth of cut on cutting force, crack initialization and propagation. The observed chip morphology highly agreed with the prediction of chip formation based on the analytical model. The curly, serrated, grainy and powdery chips formed when the cutting angle was set as 0°, 60°, 90°, and 120°, respectively. Cortical bone were removed dominantly by shearing at a small depth of cut from 10 to 50 μm, and by a mixture of pealing, shearing, fracture and crushing at a large depth of cut over 100 μm at different bone osteon angles. Moreover, its fracture toughness was calculated based on measured cutting force. It is found that the fluctuation of cutting force is suppressed and the bone material becomes easy to remove, which attributes to lower fracture toughness at bone osteon cutting angle 0°. When the cutting direction develops a certain angle to bone osteon, the fracture toughness increases then the crack propagation is inhibited to some extent and the fluctuation of cutting force comparatively decreases. There is a theoretical and practical significance for tools design and operational parameters choice in surgeries.

Keywords: Bone cutting surgery, Orthogonal cutting models, Anisotropic materials, Chip formation, Crack initialization and propagation, Fracture toughness

1 Introduction

Cortical bone cutting processes are very common in knee arthroplasties, dental implants and spine surgeries [1–3]. However, a bone cutting process exposes the risk of bone cracks. Such cracks cause an instable screw insertion [4] or instable cutting process in orthopedic robotic surgeries [5]. To predict a crack initiation and propagation, it is critical to investigate bone cutting behavior in a bone cutting process. While the cortical bone cutting behavior is a complex process due to its multi-scale structure. It consists of osteons (around 100 μm), harversian canals, interstitial lamellae, and boundaries of osteons and interstitial lamellas with the weakest bonds [6]. Therefore, the cortical bone appears an obviously anisotropic characteristic at various depths of cut and cutting directions.

Many researchers have studied three-dimensional (cutting direction across, parallel and transverse to the bone osteon orientation) bone cutting processes with the consideration of depth of cut. For example, Jacobs et al. [7] investigated how the depth of cut, tool rake angle, and bone orientation relative to cutting direction affected the chip formation to obtain in smooth and segmented chips. Malkin et al. [8] observed that the cortical bone was

*Correspondence: rebecca_ryh@hnu.edu.cn

[1] College of Mechanical and Vehicle Engineering, Hunan University, Changsha 410082, China
Full list of author information is available at the end of the article

removed as chips due to fracture occurring at the cutting edge. Sugita and Mitsuishi [9, 10] analyzed the crack propagation and proposed a cutting technique to reduce cutting force and temperature. Liao and Axinte [11] investigated the condition of a transition condition from shear to fracture of material removals in a 3D orthogonal cutting model. Feldmann et al. [12] characterized the effect of the rake angle and the depth of cut on the cutting force, the temperature and the fracture of brittle bones. Bai et al. [13] rationalized the crack propagation and chip morphology at both of microstructure and sub-microstructure scales. The aforementioned studies confined the scope of investigation for depth of cut, rake angle, and three orthogonal cutting directions. Few work was reported on the bone cutting behavior of cortical bones in more than three cutting directions. Note that in a real orthopedic surgery, not all of cutting processes are performed along an orthogonal direction. For examples, a K-wire drilling insertion was performed obliquely to orthogonal directions [14]. A drill bit design for self-centering drill on inclined plane, is neither parallel nor transverse to the bone orientation direction strictly [15]. Cseke and Heinemann [16] argued that the cutting direction affected the drilling force and chip formation. Liao et al. [17] developed a cutting model to predict cutting force and temperature subjected to a given cutting angle in bone milling. Due to anisotropy of bone materials, a slight change of the cutting angle relative to the bone orientation may alter the mechanism of chip formation and crack propagation significantly. Therefore, it is of importance to investigate cutting behaviors with a certain cutting angle other than three orthogonal directions.

To understand bone cutting behavior, the properties of cortical bone materials, in particular, fracture toughness, must be characterized. Fracture toughness describes the ability of the material in resisting crack initiation and propagation. Limited works were reported on the investigation of fracture toughness of cortical bones in orthogonal cutting: Feldmann et al. [12] presented a bone fracture toughness model when the cortical bone was cut in a perpendicular direction. Bai et al. [18] compared the bone fractures in conventional and impact cutting and found that the impact cutting was able to reduce the fracture toughness of bones. Their conclusions were based on the assumption that the cutting direction was in one of three orthogonal directions. How to affect fracture toughness in more than three directions was not covered.

This work aims to develop a cutting analytical model subjected to different orthogonal directions and large depth of cut, which includes more possibilities in range of traditional orthogonal cutting angles to simulate the real surgery situation. The calculation model of fracture toughness was further derived based on energy balance

principle to reveal the relationship between crack propagation and cutting angles in cortical bone cutting process. To validate the cutting analytical model, a series of cutting experiment was performed on fresh bovine femur bone, whose chip formation, cutting force and fracture toughness were discussed accordingly.

2 Chip Formation and Fracture Toughness in Different Bone Osteon Cutting Directions

To investigate the impact of cutting direction relative to bone osteon orientation, the cutting direction is described by a bone osteon cutting angle θ in Figure 1. In this section, in view of the anisotropic micro-structure of bone, bone osteon cutting angle θ is set as a discrete value of 0°, 60°, 90°, and 120°, respectively. The cutting scenarios are referred as mode #1, #2, #3, and #4, correspondingly. In mode #1 (Figure 1(a)), θ is set to 0°, and the cutting direction is parallel to the bone osteon orientation. In mode #2 (Figure 1(b)), θ is set to 60°, and the cutting direction is with an angle of 60° to the bone osteon orientation. In mode #3 (Figure 1(c)), θ is set to 90°, and the cutting direction is perpendicular to the bone osteon orientation. In mode #4 (Figure 1(d)), θ is set to 120°, and the cutting direction is with an angle of 120° to the bone osteon orientation.

Due to anisotropy and semi-brittle property of bones, the cortical bone is removed dominantly by shearing in a small depth of cut ranging from 10 to 60 µm. The chips are continuous in any cutting direction (Liao et al. and Bai et al. [11, 13]). Increasing the depth of cut over 100 µm, the cortical bone removal behavior will vary with the cutting direction because the bone cutting process is performed in the scale of osteons and Haversian canals. A new analytical model is needed to
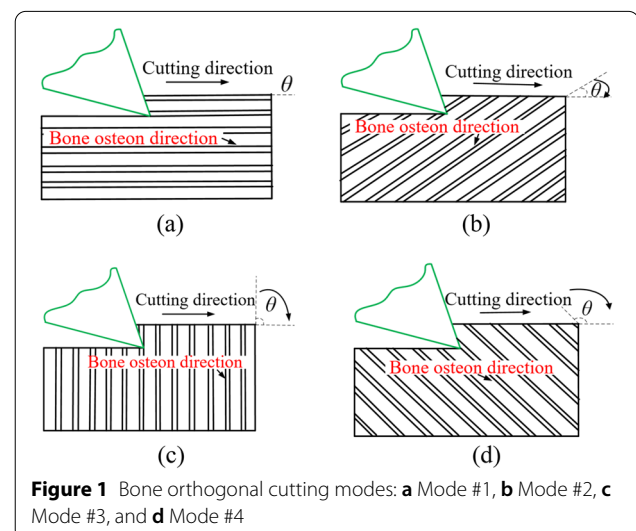

Figure 1 Bone orthogonal cutting modes: **a** Mode #1, **b** Mode #2, **c** Mode #3, and **d** Mode #4

Luo *et al. Chinese Journal of Mechanical Engineering*   (2022) 35:91

Page 3 of 12

investigate chip formation, crack initiation and propagation, cutting force, and fracture toughness in different cutting directions.

2.1 Mode #1 with a Bone Osteon Cutting Angle of 0°

In mode #1, the cutting direction is aligned with the bone osteon orientation. The cortical bone is removed along a cement line where the bone osteon and bone matrix are weakly joined. When a tool tip inserted into cortical bone with a horizontal cutting force, crack a_0 is initiated, and the crack a is stably propagated during the cutting process. The horizontal cutting force will accelerate the crack propagation along the cutting direction in Figure 2(a). The material removal is similar to peel a bone layer from the bone matrix, and the size of crack became (a_0+a).

The formed chip is simplified to a cantilever in Figure 2(b), and the chip is subjected to a bending moment by cutting forces F_n and F_c, that results in peeling a bone layer from the bone matrix. With a continuous cutting, the chip turns to a curly morphology in Figure 2(c).

A simple fracture toughness model of cortical bone is derived based on this cutting model analysis and energy balance principle. Bone material is removed by the external force applied in the tool, which converts into the elastic strain energy and potential energy for bone fracture. The elastic strain energy is equal to potential energy for bone fracture [19].

Both of vertical and horizontal cutting force F_n and F_c contribute to elastic strain energy in the cutting

Figure 2 Mode #1: **a** Cutting model, **b** Cutting force on bone osteon and **c** Predicted chip morphology

process. The elastic strain energy by F_n is found as [20, 21],

$$U_{F_n} = \frac{F_n^2(a_0 + a)^3}{2E_1 I_1}, \tag{1}$$

where E_1 is elastic modulus along to the bone osteon orientation; I_1 is the area moment of inertia calculated as,

$$I_1 = a_w h^3/12, \tag{2}$$

where h is the depth of cut, a_w is the width of cut.

The elastic strain energy by F_c is found as,

$$U_{F_c} = \frac{\left(F_c y\right)^2 (a_0 + a)}{2E I_1}, \tag{3}$$

while y is the deflection at tip related to vertical cutting force F_n as,

$$y = \frac{F_n a^2 (2a + 3a_0)}{6 E I_1}. \tag{4}$$

Therefore, the total elastic strain energy U_1 in mode #1 is found as,

$$U_1 = U_{F_c} + U_{F_n} = \frac{F_c^2 F_n^2 a^4 (2a + 3a_0)^2 (a_0 + a)}{72 E_1^3 I_1^3} + \frac{F_n^2 (a_0 + a)^3}{2E_1 I_1}. \tag{5}$$

Assuming that the required potential energy for fracture is equal to the elastic strain energy [19], fracture toughness G_1 in mode #1 is determined by the elastic strain energy as,

$$G_1 = \frac{1}{a_w} \frac{\mathrm{d} U_1(a)}{\mathrm{d} a}$$
$$= \frac{F_c^2 F_n^2 a^3 \left(28 a^3 + 96 a^2 a_0 + 105 a a_0^2 + 36 a_0^3\right)}{72 a_w E_1^3 I_1^3} + \frac{3 F_n^2 (a_0 + a)^2}{2 a_w E_1 I_1}. \tag{6}$$

The crack length is determined by [22],

$$a + a_0 = \sqrt{\frac{\pi^2 E_1 I_1}{4 F_c}}. \tag{7}$$

In Eq. (6), since a_0 or a is very small, the first part can be ignored since the polynomial powers of a_0 and a are 6. The resulted value of the first part will be insignificant in comparison with the result of the second part. Substituting Eq. (7) into Eq. (6) simplifies the expression of the fracture toughness as,

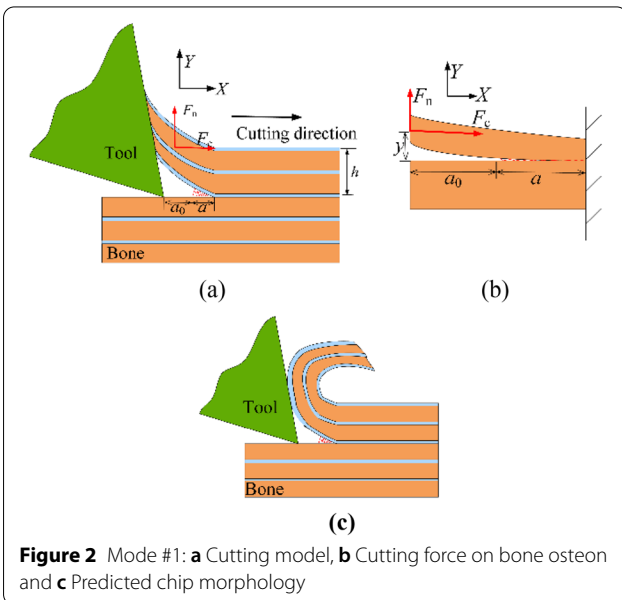$$G_1 = \frac{3\pi^2 F_n^2}{8 a_w F_c}. \tag{8}$$

Luo *et al. Chinese Journal of Mechanical Engineering*   (2022) 35:91

Page 4 of 12

Figure 3 Cutting model in mode #2

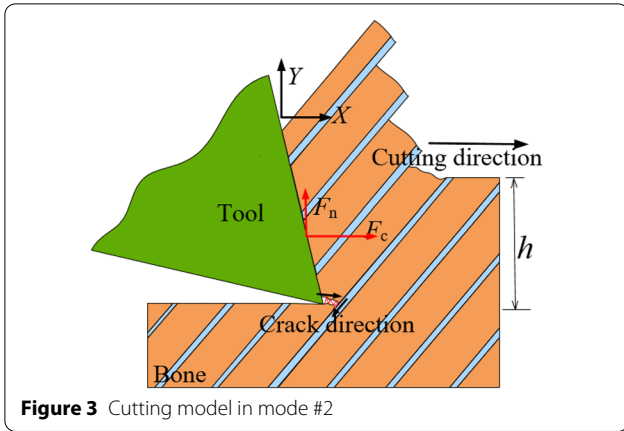**Figure 4** Mode #3: **a** Cutting model, **b** Forces applied on a bone osteon and **c** Predicted chip morphology

2.2 Mode #2 with a Bone Osteon Cutting Angle of 60°

In mode #2, the bone osteon cutting angle θ is 60°, the material is removed alone the osteon orientation due to the weak strength at the cement line. The rake face of the tool pushes and deforms the bone as serrated chips, and then the shear angle tends to close to the bone osteon cutting angle θ [23, 24]. The cortical bone is removed away at the tool tip, which is similar to the case when a ductile metal was removed in a cutting process. As shown in Figure 3, the bone chip slips along the shearing direction and deforms as serrated morphologies.

For energy conservation, the total energy was from the work by the cutting force, and it was then converted into shear energy, friction energy and fracture energy.

The condition for energy conservation was expressed by Patel et al. [25] as,

$$W = U_s + E_f + \Pi_1, \tag{9}$$

where U_s was the shear energy, E_f was the friction energy and Π_1 is the fracture energy in mode #2.

Eq. (9) could be deduced further as,

$$\frac{\sigma_s}{2}\frac{h}{\sin\theta} = \left(\frac{F_c}{a_w} - G_2\right)\cos\theta - \frac{F_n}{a_w}\sin\theta, \tag{10}$$

where σ_s is the shear stress, h is the depth of cut, a_w is the width of cut, G_2 is the fracture strength, and F_c and F_n are cutting and thrust forces, respectively.

The fracture toughness is expressed as,

$$G_2 = \frac{F_c}{a_w} - \frac{\sigma_s}{2}\frac{h}{\sin\theta\cos\theta} - \frac{F_n}{a_w}\tan\theta. \tag{11}$$

2.3 Mode #3 with a Bone Osteon Cutting Angle of 90°

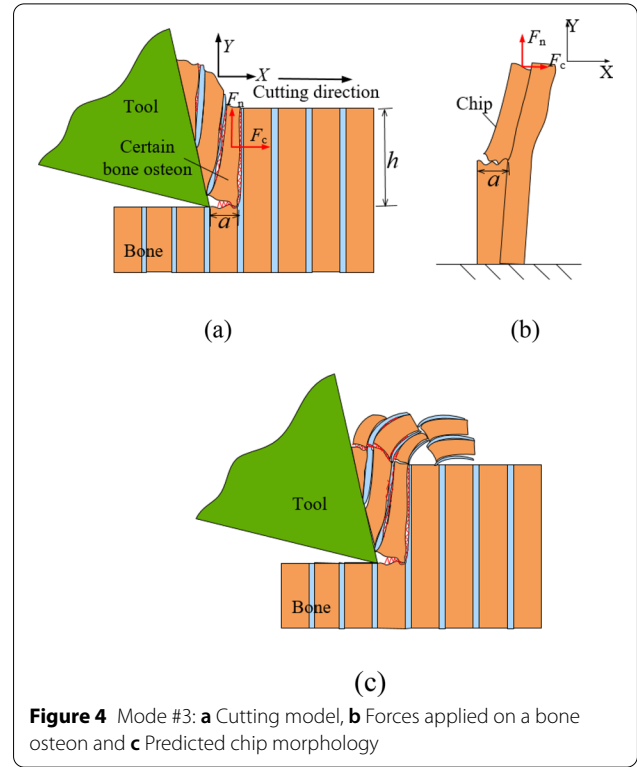The cutting direction is perpendicular to the bone osteon orientation in mode #3. The bone osteon will be bended and cracked by F_c, and the initialized crack is propagated by the effect of F_n and F_c. In Figure 4(a), bone osteons are cut down by F_c and the crack a occurs to the cutting direction. Due to a weak strength at the cement line of bone, cracks will be initialized in this boundary by the thrust force F_n. Figure 4(b) shows the cutting and thrust force that are applied on a bone osteon, the cutting force mainly cut down the bone osteon and move it one by one. The removed bone osteons turn into grainy chips that are scattered over the bone surface showed in Figure 4(c). Therefore, the chips in mode # 2 have grainy and scattered morphology. The energy conservation principle is used to analyze a fracture toughness approximately.

The elastic strain energy U_{F_n} by the thrust force is determined as [20, 21],

$$U_{F_n} = \frac{1}{2}\frac{F_n^2 h}{E_3 A} = \frac{F_n^2 h}{2E_3 A}, \tag{12}$$

where E_3 is elastic modulus of bone osteon perpendicular to the cutting direction.

While the elastic strain energy U_{Fc} by cutting force is expressed as,

$$U_{Fc} = \frac{F_c^2 h^3}{2E_3 I_3}. \tag{13}$$

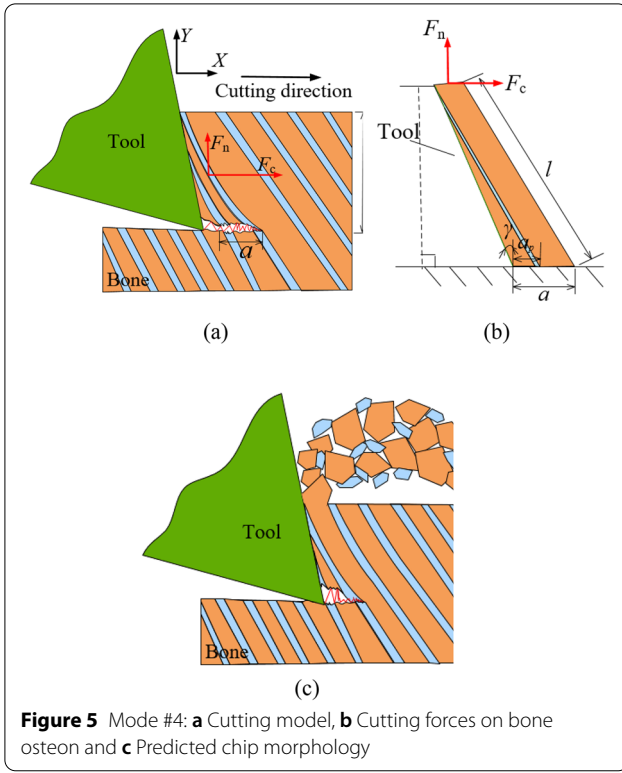The elastic strain energy U_3 is expressed as,

Figure 5 Mode #4: **a** Cutting model, **b** Cutting forces on bone osteon and **c** Predicted chip morphology

$$U_3 = U_{F_c} + U_{F_n} = \frac{F_n^2 h}{2E_3 A} + \frac{F_c^2 h^3}{2E_3 I_3}. \tag{14}$$

Similar to the case in mode #1, the fracture toughness is calculated as,

$$G_3 = \frac{U_3}{a_w a} = \frac{F_n^2 h}{2a_w a E_3 A} + \frac{F_c^2 h^3}{2a_w a E_3 I_3}, \tag{15}$$

where a is the crack length that is around the diameter d = 118 μm of bone osteon in Figure 4(b) [26], $A = d \times a_w$, $I_3 = a_w \times d^3/12$ was the area moment of inertia.

2.4 Mode #4 with a Bone Osteon Cutting Angle of 120°

In mode #4, the cutting direction is opposite to the bone osteon orientation at a 120° angle. As shown in Figure 5(a), the rake face of the tool touches the bone osteon earlier than the tool tip, and the bone osteon is bended and fractured due to the horizontal cutting force. The cutting process could be viewed to push and break bone osteons and produce the main crack a by the cutting force. Therefore, a bone osteon is modeled as a cantilever that is subjected to the cutting force.

Due to the brittleness of the bone materials, the bone osteon is crushed when the rake face made its contact. The crushed bone materials turned into powdery morphologies in cutting process in Figure 5(c).

The energy conservation principle is used to estimate the fracture toughness. The crack length a in Figure 5(b) is calculated as,

$$a_p = h[\cot(\pi - \theta) - \tan\gamma], \tag{16}$$

$$a = a_p + d, \tag{17}$$

where γ is an angle of tool rake angle.

The elastic strain energy U_{F_n} by the thrust force is found as [20],

$$U_{F_n} = \frac{F_n^2 h}{2E_4 A_4}, \tag{18}$$

where E_4 is the elastic modulus, A_4 is the area, and $A_4 = a_w \times (d+d+a_p)/2$.

The elastic strain energy U_{F_n} by the cutting force is [20],

$$U_{F_c} = \frac{F_c^2 h^3}{2E_4 I_4}, \tag{21}$$

where I_4 is the area moment of inertia of the bone osteon calculated as,

$$I_4 = \frac{a_w}{12}\left(\frac{d+d+a_p}{2}\right)^3. \tag{22}$$

Therefore, the total elastic strain energy U_4 is,

$$U_4 = \frac{F_n^2 h}{2E_4 A} + \frac{F_c^2 h^3}{2E_4 I_4}. \tag{23}$$

Finally, the fracture toughness G_4 is calculated as,

$$G_4 = \frac{U_4}{a_w a} = \frac{F_n^2 h}{2a_w a E_4 A} + \frac{F_c^2 h^3}{2a_w a E_4 I_4}. \tag{24}$$

3 Experiments

To validate the proposed cutting model in predicting chip morphology and fracture toughness in these four bone osteon cutting direction, orthogonal cutting experiments were conducted with varying cutting angles and depths of cut. The cutting tests were repeated four trials for a combination of a specified depth of cut and bone osteon cutting angle in Table 1.

Table 1 The parameters of orthogonal cutting experiments

Parameters	Value
Depth of cut h (μm)	10, 50, 90, 130
Bone osteon cutting angle θ (°)	0, 60, 90, 120

Luo *et al. Chinese Journal of Mechanical Engineering*　　(2022) 35:91

Page 6 of 12

Due to the similar properties to human bones, bovine femur bones were commonly used in bone cutting experiments [[27]]. To prepare bone osteons for a cutting angle of 60° or 120°, fresh bovine femur bones were sawed to small pieces manually. Pieces were then grounded to produce bone blocks with an inclined face of a 60° angle. As shown in Figure 6(a), three machined faces were named as Face #1, #2 and #3, respectively. In each mode, the face with corresponding bone osteon orientation was set as cut face. To meet the condition of orthogonal cutting, the width of the cutter was wider than the width of bone sample. Thus, the bone block was sliced with a width of 1.5 mm in parallel to Face #1, #2 and #3, respectively. The tool had a width of 2 mm in Figure 6(b). The prepared bones were stored in refrigerator.

To acquire stable cutting forces and chip morphologies in four modes with a different depth of cut, a micro-cutting setup was used to perform orthogonal cutting experiments in Figure 6(c). Two active linear stages (Y axis and Z axis) (Model 200cri, Siskiyou Instrument) were mounted on the third active linear stage (X axis) (Model HLD 60, Moog Animatics). A precision micro-linear stage (Z' axis) (Model Micro-Controle, Klinger) was mounted on the Z axis linear stage to provide precise feeding. The tool (Thinbit) had its rake and rear angles of 10° and 15°, respectively. It was clamped on the precision Z' axis to conduct these experiments. The cutting speed was set as 0.5 mm/s. A prepared bone was taken from the refrigerator and immersed into the saline for 2 h at room temperature, and was then clamped on the worktable by a step block clamp.

In addition, the micro-cutting system was equipped with (1) a piezoelectric dynamometer (Model 9256C, Kistler) to measure cutting forces, (2) a data recorder (Model DL750 ScopeCorder, Yokogawa) to record force data with the sampling rate of 2000 Hz, and (3) a digital microscope (Model 503+, Gaosuo) to catch chip morphologies under different cutting conditions as shown in Figure 6(c).

4 Experimental Results
4.1 Chip Morphologies
Figure 7 showed the variety of chip morphologies in mode #1 ($\theta = 0°$): Figure 7(a) showed a continuous chip in a spiral shape under the depth of cut of 10 μm. Figure 7(b) showed a continuous chip in a curvy shape under the depth of cut of 50 μm. Figure 7(c) showed a serrated chip under the depth of cut of 90 μm, and Figure 7(d) showed a much curlier chip under the depth of cut of 130 μm.

Figure 8 showed various chip morphologies in mode #2 ($\theta = 60°$): Figure 8(a) showed continuous chip shape, but the curly chip was not like Figure 7(a) with a spiral curly chip. With the increase of depth of cut (50 μm, 90 μm and 130 μm), it always showed a serrated chip, but its morphology is from slightly serrated to severely serrated in Figures 8(b), (c) and (d).

When the cutting direction was perpendicular to the bone osteon orientation, Figure 9(a) showed the continuous chip under the depth of cut of 10 μm. The chip became serrated when the depth of cut was set as 50 μm in Figure 9(b). The chip became discontinued when
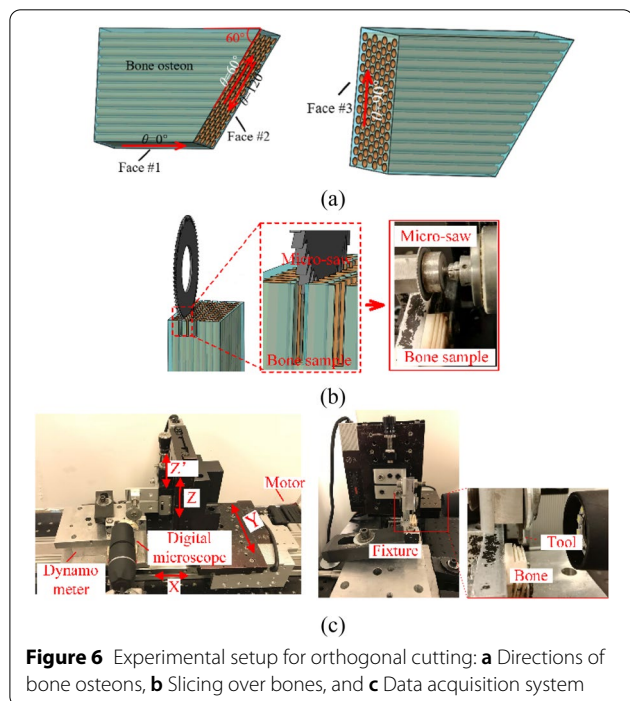
Figure 6 Experimental setup for orthogonal cutting: **a** Directions of bone osteons, **b** Slicing over bones, and **c** Data acquisition system
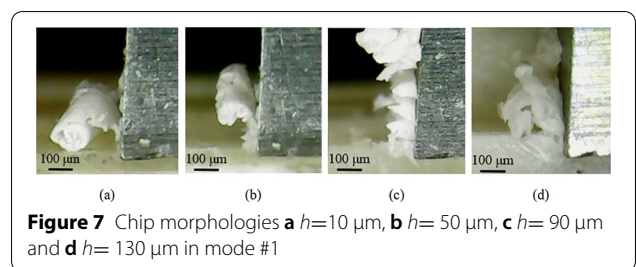
Figure 7 Chip morphologies **a** h=10 μm, **b** h= 50 μm, **c** h= 90 μm and **d** h= 130 μm in mode #1
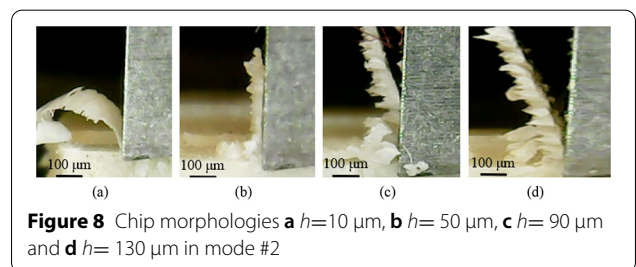
Figure 8 Chip morphologies **a** h=10 μm, **b** h= 50 μm, **c** h= 90 μm and **d** h= 130 μm in mode #2
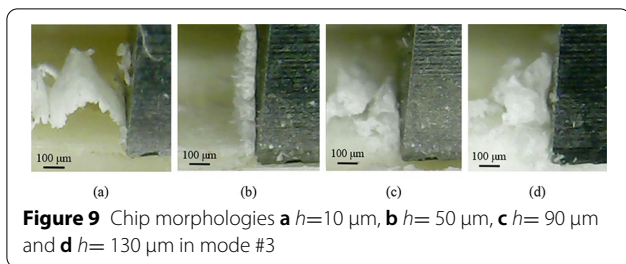
Figure 9 Chip morphologies **a** $h=10$ μm, **b** $h=50$ μm, **c** $h=90$ μm and **d** $h=130$ μm in mode #3
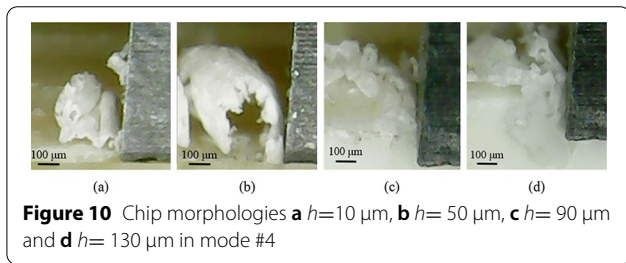
Figure 10 Chip morphologies **a** $h=10$ μm, **b** $h=50$ μm, **c** $h=90$ μm and **d** $h=130$ μm in mode #4

Figure 11 Cutting forces with the depth of cut of 10 μm: **a** Mode #1, **b** Mode #2, **c** Mode #3, and **d** Mode #4

the depth of cut was set as 90 μm in Figure 9(c). At the depth of cut of 130 μm, the chip became large grainy as shown in Figure 9(d).

When the bone osteon cutting angle was set as 120°, the cutting direction was opposite to the bone osteon orientation. With a depth of cut of 10 μm, the chip in Figure 10(a) was still continuously but tended to be broken easily. With a depth of cut of 50 μm, the chip in Figure 10(b) became continuous. With a depth of cut larger than 90 μm, the chips in Figures 10(c) and (d) were crushed to powdery morphology.

4.2 Cutting Force

Figure 11 showed the cutting forces when the depth of cut was set as 10 μm in four cutting modes. Figures 11(a) and (b) showed that the horizontal and vertical cutting forces in mode #1 and 2 were relatively stable; while the cutting forces in Figures 11(c) and (d) for mode #3 and 4 showed obvious fluctuating.

Figure 12 showed the cutting forces when the depth of cut was set as 130 μm in four cutting modes. A cutting force was characterized as its static and amplitude components. Although the static horizontal cutting force in any of these four modes remained constant, the amplitude of horizontal cutting force was increased when the cutting angle was increased from Figures 12(a) to (d).

Figure 13 compared the static horizontal and vertical cutting forces in different depths of cut. The solid lines were fitted by linear least squares. From the scatter dots in the depth of cut of 10 μm, the mean horizontal forces exhibited the same changing trend and increased with an increase of the cutting angle or the depth of cut shown
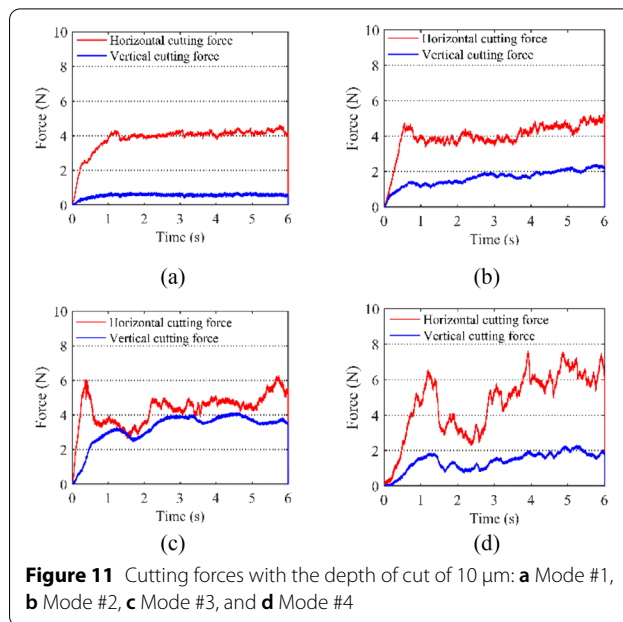

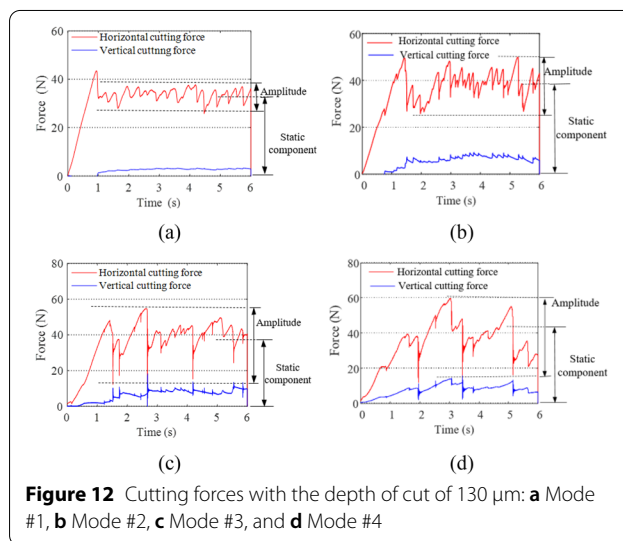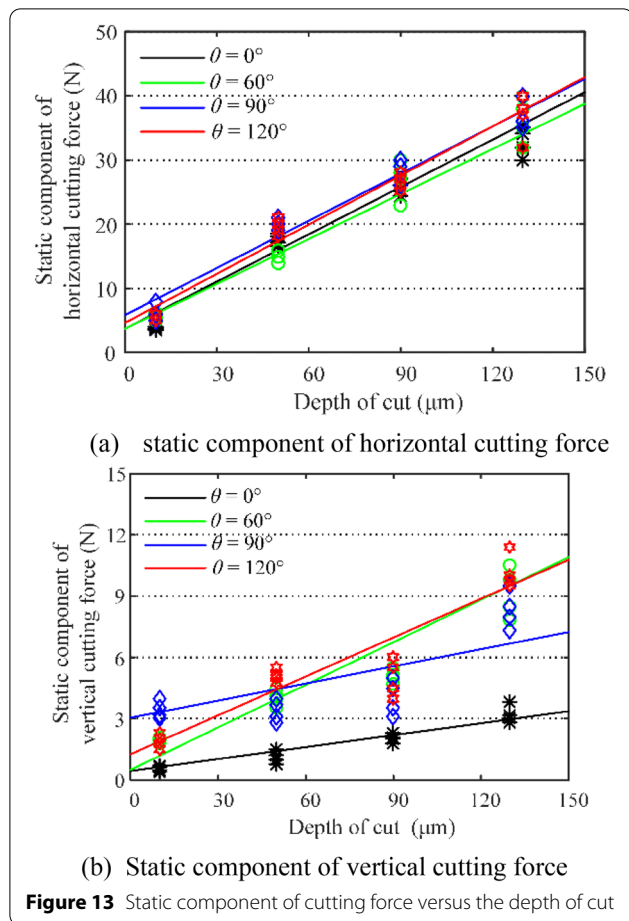**Figure 12** Cutting forces with the depth of cut of 130 μm: **a** Mode #1, **b** Mode #2, **c** Mode #3, and **d** Mode #4

in Figure 13(a). The depth of cut and cutting angle also affect the static vertical cutting forces significantly as shown in Figure 13(b).

4.3 Fracture Toughness

The bone fracture toughness could be calculated based on the static components of cutting force from bone orthogonal cutting experiments in four modes. The elastic modulus in different bone osteon cutting angles is listed in Table 2. The shear stress σ_s in bone osteon cutting angle 60° is 6.7×10^7 N/m^2 [28]. Thus, according to Eqs. (8), (11) and (22) the values of fracture toughness

Luo *et al. Chinese Journal of Mechanical Engineering*   (2022) 35:91

Page 8 of 12

(a)   static component of horizontal cutting force

(b)   Static component of vertical cutting force

Figure 13 Static component of cutting force versus the depth of cut

in different bone osteon cutting angles are calculated to 652 ± 184 N/m, 3105 ± 1310 N/m, 1695 ± 302 N/m and 1532 ± 149 N/m, respectively.

5 Discussion

When the depth of cut was set as 10 μm, there are continuous chips in cutting process at four bone osteon cutting angles. The cortical bone is removed by shearing during depth of cut in the bone fibrils arrays scale [5]. But these chips show a very small radius and tight curl morphology at bone osteon cutting angle 0°. At bone osteon cutting angle 60°, chips show a larger radius and stretches forward. At bone osteon cutting angle 90°, chips show a continuous morphology at tool tip and curl forward until

breaking down. At bone osteon cutting angle 120°, chips show a small radius and easily break down. Due to anisotropy of cortical bone, these differentiated chip morphology phenomena attributes to different fracture strains of chips at four bone osteon cutting angles.

When the depth of cut is smaller than 20 μm, the horizontal cutting force is stable with less fluctuating shown in Figures 11(a) and (b). However, the cutting angle affects the fracture in sense that the tool needs to cut down the bone osteon in a transverse or even slightly opposite direction, this explained the light vibrations of horizontal cutting forces in Figures 11(c) and (d).

When the depth of cut was increased to 50 μm, the serrated chip indicates that the material is removed by shearing. This result agrees well with the conclusion in Refs. [11, 13] that the serrated chip happens when the depth of the cut was in the range of 20 μm to 60 μm. Based on the experimental results and theoretical models, shearing become the dominating material removal behavior when the depth of cut is set in this range. The bone osteon orientation mainly affects curling of chips and slightly affects the horizontal cutting force.
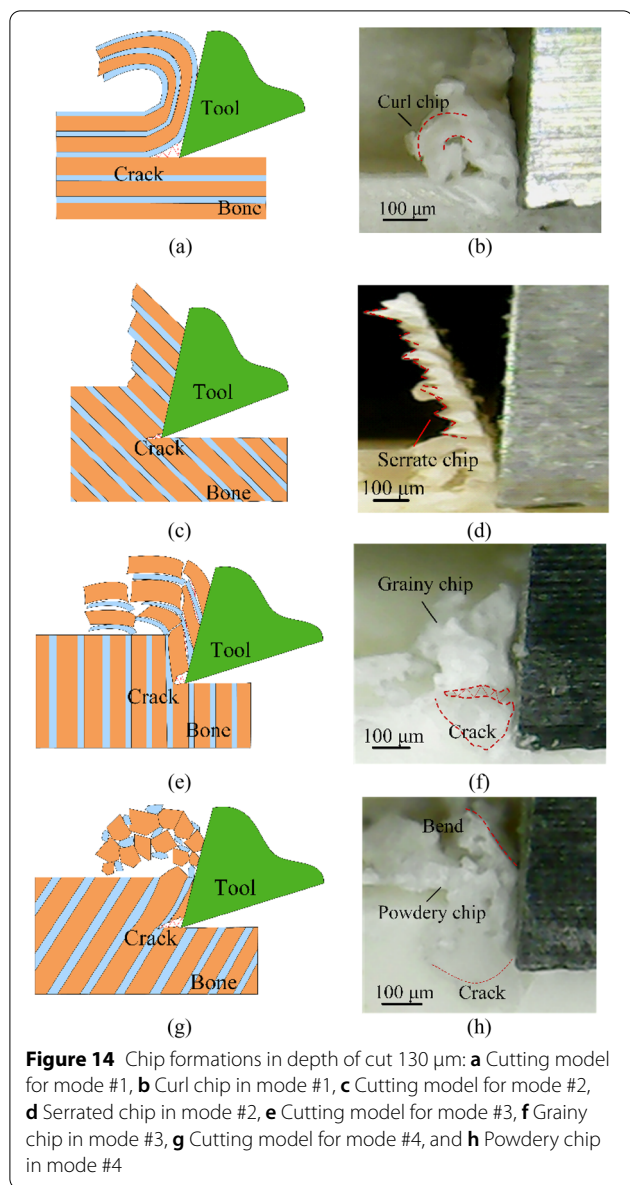
When the depth of cut was set over 100 μm, the cortical bone cutting behaviors were highly diversified. Taking an example of mode #1, a layered chip should be formed along bone osteon direction when the depth of cut (such as 130 μm) is at the scale of the diameters of osteons or Haversian canals (in Figure 14(a)) from the analytical model. Fortunately, a layered and curled bone chip was observed on the tool rake face in Figure 14(b). This bone removal behavior in this mode #1 could be viewed as peeling layered bone from the bulk materials. It could generate a high quality surface along this direction due to the curl chip formation (in Figure 14(b)) and stable force figure with time (in Figure 12(a)) [29].

In mode #2, the cutting angle affects the cutting behaviors significantly. The material is removed by shearing, which is totally different from the peeling behavior in mode #1. The serrated chip was observed since the tilted bone osteon formed a shear angle with the cutting direction. The rake face pushes the chip forward, meanwhile the materials are squeezed to make itself continuously stretched with the cutting process continuing. The chip develops serrated chip as shown in Figure 14(d).

In mode #3, the bone osteon cutting angle was set to 90°. On the one hand, the horizontal cutting force that

Table 2 Elastic modulus in different bone osteon orientations [28]

Parameter	Value			
Bone osteon cutting angle θ (°)	0	60	90	120
Elastic modulus ($\times 10^9$ N/m^2)	10.4 ± 1.64	12.8 ± 1.57	23.1 ± 3.18	12.8 ± 1.57

Figure 14 Chip formations in depth of cut 130 μm: **a** Cutting model for mode #1, **b** Curl chip in mode #1, **c** Cutting model for mode #2, **d** Serrated chip in mode #2, **e** Cutting model for mode #3, **f** Grainy chip in mode #3, **g** Cutting model for mode #4, and **h** Powdery chip in mode #4

Figure 14(f) matched the results of theoretical analysis reported in Ref. [10]. Therefore, cortical bone is removed in mode #3 by fracture and formed grainy chips.
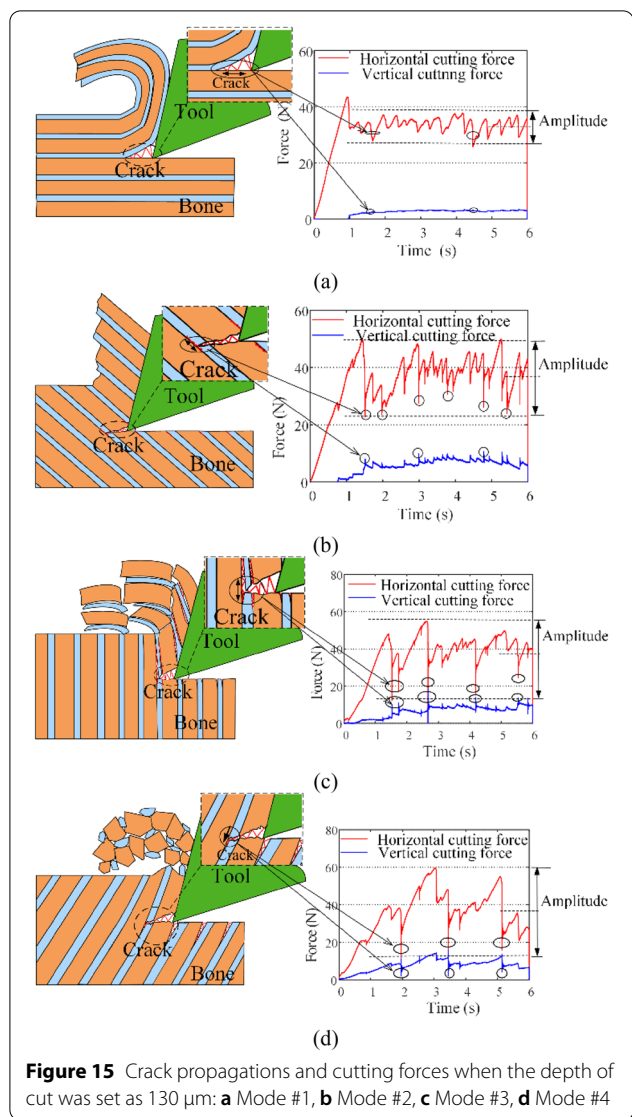
In mode #4, the bone material removal process experiences bending and crushing simultaneously (Figure 14(g)) when the bone osteon cutting angle was set as 120°. Different from the bone removal behavior in mode #3, the rake face of tool touches the bone osteon earlier than the tool tip. The rake face of cutting tool produces a press on the bone osteon, and then the tool tip generates a contact to bone osteon in proceeding the cutting process. The chip is crushed to power morphology as shown in Figure 14(h).

For the bone fracture toughness in mode #1, although the bone chip is peeling from the bone matrix, the material is fractured by an open mode [19]. While the fracture toughness was calculated to 652 ± 184 N/m. It is fairly close to the reported reference value 644 ± 102 N/m in Table 3. At present, few work reports the fracture toughness at bone osteon cutting angle 60°. For mode #2, it belongs to the shear mode fracture based on the analysis model of bone chip formation (Figure 3). According to Ref. [30], at bone osteon cutting angle 0° and 90° the reference value of fracture toughness is 1723 ± 487 N/m and 4710 ±1284 N/m, respectively, in Table 3. According to Eq. (11), calculated value of fracture toughness is 3105 ± 1310 N/m at bone osteon cutting angle 60°, which is just within scope of the above reference value. In mode #3, the crack is produced perpendicularly to the bone osteon orientation, the fracture mechanism is an open mode, and the corresponding fracture toughness was 1495 ± 302 N/m. The deviation of fracture toughness is large since the cutting force is fluctuated sharply. The estimated fracture toughness is similar to the reported value 1532±149 N/m [30]. In mode #4, few work is reported for the corresponding fracture toughness. Since the cutter is slightly opposite to the bone osteon orientation, the required cutting energy in this mode is larger than that in mode #3. The fracture toughness in model #4 was slightly larger than that in mode #3.

The largest fracture toughness was mode #2 in a shear mode fracture, followed by mode #4, mode #3, and mode #1 in open mode fracture. Figure 15 showed the correspondence of crack growth and propagation and amplitude of cutting force. The fracture toughness is associated

mainly applies in the bone osteon to produce the main crack (Figure 4(c)). On the other hand, the vertical cutting force makes the cortical bone to produce a crack along the cement line with a weakest strength. So the grainy chips are generated (Figure 14(e)). The experimental result showed that the chip morphology in

Table 3 Fracture toughness value

Fracture toughness		Bone osteon cutting angle			
		0°	60°	90°	120°
Calculated value (N/m)		652 ± 184	3105 ± 1310	1495 ± 302	1532 ± 149
Reference value (N/m) [[30]]	Open mode	644 ± 102	–	1374 ± 183	–
	Shear mode	2430 ± 836	–	4710 ± 1284	–

Luo *et al. Chinese Journal of Mechanical Engineering*   (2022) 35:91

Page 10 of 12

Figure 15 Crack propagations and cutting forces when the depth of cut was set as 130 μm: **a** Mode #1, **b** Mode #2, **c** Mode #3, **d** Mode #4

with crack initiation and propagation. The lowest fracture toughness was mode #1. It meant that the crack easily propagated in mode #1. The crack is along the weak cement line in the cutting direction, and it produces a stable cutting force (see the enlarged view in the right of Figure 15(a)). For the shear mode fracture in mode #2, the crack is propagated hardly down to the next cement line of bone, because this bone osteon bears a shear force obliquely up to the next osteon. A long and deep micro crack cannot be produced in the next cement line, as arrowed shown in the left of Figure 15(b). But a tiny micro crack could occur due to the vertical cutting force. Since the micro cracks propagated speed is faster than cutting speed, when the tool tip approached nucleation location of micro crack, a vibration force occurs (see the enlarged view in the right of Figure 15(b)). In mode #3, the crack is initialized and propagated to the next bone

osteon in advance. The direction of the crack propagation is perpendicular to the cutting direction as arrowed in the left side of Figure 15(c). When the cutter arrives here, it produces a highly vibrated cutting force (see the enlarged view in the right of Figure 15(c)), the amplitude of the horizontal force is larger than that in Figure 15(b). Since the fracture toughness is smaller than that in mode #2, it easily produces a vertical crack to the cutting direction. In mode #4, a crack propagates to the next bone osteon and then extends along the weak cement line, which is stretched in machined surface deeply. Since the rake face of tool touches the bone osteon with a horizontal force. This horizontal force accelerates the crack propagation along the cement line along the arrow shown in the left of Figure 15(d). When the tool arrives here, it produces more highly vibrated force (see the enlarged view in the right of Figure 15(d)).

In a summary, when the fracture toughness is small, and the crack is initialized and propagated along the cutting direction, it would produce a stable cutting force and result in high quality surface. In such an operating condition, the crack helps the material removal process. When the crack growth and propagation is not along the cutting direction, the fracture toughness is increased to suppress crack propagation, then it will produce a comparatively stable cutting force.

6 Conclusions

This work was motivated to optimize cutting parameters to suppress vibration and avoid undesired fracture in precise cutting processes in surgeries. In particular, the impact of the depth of cut and the cutting direction relative of bone osteon orientation on chip formation and fracture toughness were focused. The analytical models for four typical conditions were developed, and experiments were performed to show the effectives of the proposed models in predicting chip morphologies and cutting forces. It has been found that:

(1) The chip morphology is affected by the cutting direction relative to the bone osteon orientation and the depth of cut greatly. With a small depth of cut, the chip is continuous, and the curl radius of chip varied with the cutting angle. With a large depth of cut, the chip morphology become curly, serrate, grainy and powdery when the cutting angle is set as 0°, 60°, 90°, and 120°, respectively.

(2) The proposed cutting models and experimental results showed that the cortical bone cutting behavior is varied with the depths of cut and the cutting direction. In a small depth of cut up to 50 μm, the cortical bone is removed by shearing, and the

impact of the cutting angle is insignificant. When the depth of cut reached over 130 μm, the bone osteon cutting angle affects the cutting behavior greatly, and the materials are removed by peeling, shearing, fracture, and a mixture of bending and crushing at the cutting angle of 0°, 60°, 90°, and 120°, respectively.

(3) For a large depth of cut, the fracture toughness model was established and applied to estimate the fracture toughness under a varying angle. Using the acquired cutting force data from experiments, the calculated fracture toughness was found as 652 ± 184 N/m, 3105 ± 1310 N/m, 1495 ± 302 N/m and 1532 ± 149 N/m at the cutting angle of 0°, 60°, 90°, and 120°, respectively.

(4) The interior crack of bone always propagates along the bone cement line with a weakest strength. When the cutting direction (bone osteon cutting angle 0°) corresponds to the direction of the bone cement line, the fracture toughness of bone appears relatively low. The crack propagates very easily, that contributes to removing bone material. When the cutting direction develops a certain angle (bone osteon cutting angle 60°, 90° and 120°) to the bone cement line, in other words develops a certain angle to the direction of crack propagation, the fracture toughness appears large. Therefore, in this situation it need more energy to remove material. The crack propagation is inhibited and the cutting force becomes relatively stable.

The aforementioned findings have this theoretical and practical significance in helping engineers to design orthopedic tools and optimize operational parameters in bone-cutting surgeries.

Abbreviations
a: Crack length; a_o: Initial crack length; a_p: Crack length of cutter to first bone osteon; a_w: Width of cut; A_1: Cross-sectional area in mode #1; A_4: Cross-sectional area in mode #4; d: Diameter of single bone osteon; E_1: Elastic modulus in mode #1; E_2: Elastic modulus in mode #2; E_3: Elastic modulus in mode #3; E_4: Elastic modulus in mode #4; E_f: Friction energy; F_c: Horizontal cutting force; F_n: Vertical cutting force; G_1: Fracture toughness in mode #1; G_2: Fracture toughness in mode #2; G_3: Fracture toughness in mode #3; G_4: Fracture toughness in mode #4; h: Depth of cut; I_1: Area moment of inertia in mode #1; I_3: Area moment of inertia in mode #3; I_4: Area moment of inertia in mode #4; M: Moment of force; U_1: Elastic strain energy in mode #1; U_s: Shear energy in mode #2; U_3: Elastic strain energy in mode #3; U_4: Elastic strain energy in mode #4; U_{Fn}: Elastic energy produced by F_n; U_{Fc}: Elastic energy produced by F_c; W: Work by external force; y: A deflection in mode #1; θ: Bone osteon cutting angle; γ: Tool rake angle; σ_s: Shear stress; σ_c: Stress in cutting direction; π_2: Fracture energy.

Author contributions
YL and YR designed experiments, acquired data and edited manuscript draft; Y S assisted with experiments data analysis; CM, ZZ and ZB edited and supervised the manuscript. All authors read and approved the final manuscript.

Authors' Information
Yuanqiang Luo, born in 1990, is currently a lecturer at *College of Automotive and Mechanical Engineering, Changsha University of Science and Technology,* China. She received her PhD. Degree from *Hunan University, China*, in 2020. Her research interests include bio-material processing technology and medical device manufacturing. Tel: +86-18229975357; E-mail: yuanqial@csust.edu.cn.
Yinghui Ren, born in 1979, is currently an associate professor at *College of Mechanical and Vehicle Engineering, Hunan University, China*. She received her PhD. degree from *Hunan University, China*, in 2009. Her research interests include precision processing technology and medical device manufacturing. Tel: +86-13548596452; E-mail: rebecca_ryh@hnu.edu.cn.
Yang Shu, born in 1990, is currently a PhD candidate at *College of Mechanical and Vehicle Engineering, Hunan University, China*. His research interests include precision machining and intelligent molding. Tel: +86-15675124936; E-mail: yshu@hnu.edu.cn.
Cong Mao, born in 1975, is currently a professor at *College of Automotive and Mechanical Engineering, Changsha University of Science and Technology, China*. He received his PhD. degree from *Hunan University, China*, in 2008. His research interests include precision processing technology of difficult-to-cut materials. Tel: +86-731-85258630; E-mail: maocong315@aliyun.com.
Zhixiong Zhou, born in 1953, is currently a professor at *College of Mechanical and Vehicle Engineering, Hunan University, China*. E-mail: zhouzx8@hnu.edu.cn.
Z.M. Bi, born in 1975, is currently a professor at *Department of Civil and Mechanical Engineering, Purdue University Fort Wayne, U.S.A*. His research interest includes precision processing technology. E-mail: biz@pfw.edu.

Availability of data and materials
The datasets supporting the conclusions of this article are included within the article.

Competing interests
The authors declare no competing financial interests.

Author Details
[1]College of Mechanical and Vehicle Engineering, Hunan University, Changsha 410082, China. [2]Hunan Provincial Key Laboratory of Intelligent Manufacturing Technology for High-performance Mechanical Equipment, Changsha University of Science and Technology, Changsha 410114, China. [3]Department of Civil and Mechanical Engineering, Purdue University Fort Wayne, Fort Wayne, IN 46805, USA.

References
[1] D Axinte, Y B Guo, Z R Liao, et al. Machining of biocompatible materials – recent advances. *CIRP Annals – Manufacturing Technology*, 2019, 68: 629–652.
[2] Z H Chen, Y Zhang, C Y Wang, et al. Understanding the cutting mechanisms of composite structured soft tissues. *International Journal of Machine Tools and Manufacture*, 2020, 161(3):103685.
[3] J A Robles-Linares, D Axinte, Z R Liao, et al. Machining-induced thermal damage in cortical bone: Necrosis and micro-mechanical integrity. *Materials and Design*, 2021, 197:109215.
[4] M Hollensteiner, S Sandriesser, E Bliven, et al. Biomechanics of osteoporotic fracture fixation. *Current Osteoporosis Report*, 2019, 17: 363–374.
[5] L Bai, J X Yang, X H Chen, et al. Medical robotics in bone fracture reduction surgery: A review. *Sensors*, 2019, 19: 3593-3612.

[6] E A Zimmermann, M E Launey, R O Ritchie. The significance of crack-resistance curves to the mixed-mode fracture toughness of human cortical bone. *Biomaterials*, 2010, 20(31): 5297–5305.

[7] C H Jacobs, M H Pope, J T Berry, et al. A study of the bone machining process-orthogonal cutting. *Journal of Biomechanics*, 1974, 7: 131–136.

[8] K L Wiggins, S Malkin. Orthogonal machining of bone. *Journal of Biomechanics Engineering*, 1978, 100(3): 122-130.

[9] N Sugita, M Mitsuishi. Specifications for machining the bovine cortical bone in relation to its microstructure. *Journal of Biomechanics*, 2009, 42(16): 2826–2829.

[10] N Sugita, T Osa, R Aoki, et al. A new cutting method for bone based on its crack propagation characteristics. *CIRP Annal - Manufacturing Technology*, 2009, 58(1): 113–118.

[11] Z R Liao, D A Axinte. On chip formation mechanism in orthogonal cutting of bone. *International Journal of Machine Tools and Manufacture*, 2016, 102: 41–55.

[12] A Feldmann, P Ganser, L Nolte, et al. Orthogonal cutting of cortical bone: Temperature elevation and fracture toughness. *International Journal of Machine Tools and Manufacture*, 2017, 118–119: 1–11.

[13] W Bai, L M Shu, R L Sun, et al. Mechanism of material removal in orthogonal cutting of cortical bone. *Journal of Mechanical Behavior of Biomedical Materials*, 2020, 104.

[14] S A Brennan, C Kiernan, S Beecher, et al. Volar plate versus k-wire fixation of distal radius fractures. *Injury*, 2016, 47: 372–376.

[15] L M Shu, S H Li, M Terashima, et al. A novel self-centring drill bit design for low-trauma bone drilling. *International Journal of Machine Tools and Manufacture*, 2020, 154.

[16] A Cseke, R Heinemann. The effects of cutting parameters on cutting forces and heat generation when drilling animal bone and biomechanical test materials. *Medical Engineering and Physics*, 2018, 51: 24–30.

[17] Z R Liao, D Axinte, D Gao. On modelling of cutting force and temperature in bone milling. *Journal of Materials Processing Technology*, 2019, 266: 627–638.

[18] W Bai, L M Shu, R L Sun, et al. Improvements of material removal in cortical bone via impact cutting method. *Journal of Mechanical Behavior of Biomedical Materials*, 2020, 108.

[19] T L Anderson. *Fracture mechanics: fundamentals and application*. 3rd ed. USA: CRC Press, 2005.

[20] Y Huang, H Z Lin, Y N Wang, et al. *Mechanics of materials*. China: Science Press, 2016. (in Chinese)

[21] O G Diaz, D A Axinte. Towards understanding the cutting and fracture mechanism in ceramic matrix composites. *International Journal of Machine Tools and Manufacture*, 2017, 118–119: 12–25.

[22] L X Chen, K F Zhang, H Cheng, et al. A cutting force predicting model in orthogonal machining of unidirectional CFRP for entire range of fiber orientation. *The International Journal of Advanced Manufacturing Technology*, 2017, 89: 833–846.

[23] H Li, X D Qin, G Y He, et al. Investigation of chip formation and fracture toughness in orthogonal cutting of UD-CFRP. *The International Journal of Advanced Manufacturing Technology*, 2016, 82: 1079–1088.

[24] R O Ritchie, M J Buehler, P Hansma. Plasticity and toughness in bone. *Physics Today*, 2009, 62: 41–47.

[25] Y Patel, B R K Blackman, J G Williams. Determining fracture toughness from cutting test on polymers. *Engineering Fracture Mechanics*, 2009, 76: 2711–2730.

[26] J P Morales, H I Roa, D Zavando, et al. Determination of the species from skeletal remains through histomorphometric evaluation and discriminant analysis. *International Journal of Morphology*, 2012, 30: 1035–1041.

[27] P Geoeges, P Squire. Comparison of the mechanical properties of a new bone xenograft with human and bovine trabecular bone. *Orthopedie Traumatologie*, 1992, 2(4): 265–268.

[28] D T Reilly, A H Burstein. The elastic and ultimate properties of compact bone tissue. *Journal of Biomechanics*, 1975, 8: 393–493.

[29] P L Huang, J F Li, J Sun, et al. Vibration analysis in milling titanium alloy based on signal processing of cutting force. *The International Journal of Advanced Manufacturing Technology*, 2013, 64: 613–621.

[30] Z D Feng, J Rho, S Han, et al. Orientation and loading condition dependence of fracture toughness in cortical bone. *Materials Science and Engineering:C*, 2000, 11(1): 41–46.